REVIEW ARTICLE | NOVEMBER 04 2022

A comprehensive review of computational and image analysis techniques for quantitative evaluation of striated muscle tissue architecture

Tessa Altair Morris; Sarah Eldeen; Richard Duc Hien Tran; ... et. al

Biophysics Rev. 3, 041302 (2022)
https://doi.org/10.1063/5.0057434

Biophysics Reviews REVIEW scitation.org/journal/bpr

A comprehensive review of computational and image analysis techniques for quantitative evaluation of striated muscle tissue architecture

Cite as: Biophysics Rev. 3, 041302 (2022); doi: 10.1063/5.0057434
Submitted: 20 May 2021 · Accepted: 3 October 2022 ·
Published Online: 4 November 2022

Tessa Altair Morris,[1,2,3] Sarah Eldeen,[1] Richard Duc Hien Tran,[2,4] and Anna Grosberg[1,2,3,4,5,6,a)]

AFFILIATIONS

[1]Center for Complex Biological Systems, University of California, Irvine, California 92697-2700, USA
[2]UCI Edwards Lifesciences Foundation Cardiovascular Innovation and Research Center (CIRC), University of California, Irvine, California 92697-2700, USA
[3]NSF-Simons Center for Multiscale Cell Fate Research, University of California, Irvine, California 92697-2700, USA
[4]Department of Biomedical Engineering, University of California, Irvine, California 92697-2700, USA
[5]Department of Chemical and Biomolecular Engineering, University of California, Irvine, California 92697-2700, USA
[6]Sue and Bill Cross Stem Cell Research Center, University of California, Irvine, California 92697-2700, USA

[a)]Author to whom correspondence should be addressed: grosberg@uci.edu

ABSTRACT

Unbiased evaluation of morphology is crucial to understanding development, mechanics, and pathology of striated muscle tissues. Indeed, the ability of striated muscles to contract and the strength of their contraction is dependent on their tissue-, cellular-, and cytoskeletal-level organization. Accordingly, the study of striated muscles often requires imaging and assessing aspects of their architecture at multiple different spatial scales. While an expert may be able to qualitatively appraise tissues, it is imperative to have robust, repeatable tools to quantify striated myocyte morphology and behavior that can be used to compare across different labs and experiments. There has been a recent effort to define the criteria used by experts to evaluate striated myocyte architecture. In this review, we will describe metrics that have been developed to summarize distinct aspects of striated muscle architecture in multiple different tissues, imaged with various modalities. Additionally, we will provide an overview of metrics and image processing software that needs to be developed. Importantly to any lab working on striated muscle platforms, characterization of striated myocyte morphology using the image processing pipelines discussed in this review can be used to quantitatively evaluate striated muscle tissues and contribute to a robust understanding of the development and mechanics of striated muscles.

TABLE OF CONTENTS

I. INTRODUCTION

Striated muscle is an integral part of both the heart and skeletal muscle, and its proper function is essential for survival. The emergent

function of striated muscle organs is influenced by architecture at multiple length scales (Fig. 1). The appearance of striated muscle is derived from the alternating pattern of thick myocin filaments and thin actin filaments [Figs. 1(a)–1(c)].[1] In a longitudinal section through myofibrils, an array of myofilaments, alternating, anisotropic dark bands appear, which are called z-lines or z-discs [Figs. 1(b)–1(d)], and the area between two z-lines is called a sarcomere [Fig. 1(b)].[1] Striated muscle utilizes the synchronized contraction of sarcomeres organized at the multiple length scales to properly function,[1] which in the heart, leads to forces that can pump blood throughout the body. As a result, any structural changes within the architecture of the myocardium leading to impaired cardiac function.[2] Recreating *in vitro* the normal and pathological *in vivo* architecture would significantly improve our understanding of the mechanisms that link the architecture of the striated muscle and the emergent function. To achieve this, it is essential to be able to quantify the multi-scale architecture of proteins and cells that compose the striated muscle tissues.[7] However, the multitude of different proteins in the striated muscle (actin, α-actinin, tubulin, etc.) that is part of different constructs such as myofibrils [Fig. 1(c)], z-lines, and microtubules create a challenge in the analysis and quantitative description of architecture.

Quantification of cellular morphology and structure from images is fundamental to the study of striated muscles. It has been used to characterize muscle developmental stages,[3–5] engineered tissues,[6–10] effects of disease[11–14] or injury,[15–18] and treatment with pharmacological agents[19] as well as to predict the reduction in contractile function.[2,20,21] This is in large part due to the unique link between structure and function in striated myocytes, as their ability to contract is dependent on the nearly crystalline order of their cytoskeletal components.[22,23] Indeed, a large fraction of human myopathies is the result of mutations in the structural components.[23] While many of the hypotheses about the aspects of striated myocyte morphology that impact function may come from the qualitative assessment of images, it is essential to use quantitative techniques to ensure reproducibility and reliability across labs, which is especially challenging for immature and highly variable cell types.

These new cell types have emerged as the adult heart has a restricted regenerative potential because the mature cardiomyocytes (CMs) are at the post-mitotic stage, making the heart vulnerable to progressive damage. A couple of strategies, used to supplement existing cardiac cells, are (1) forcing cardiac cells back into a pre-mitotic stage,[24] and (2) using stem-cell derived cardiomyocytes.[2] The development of human-induced pluripotent stem-cell-derived cardiomyocytes (hiPSC-CMs) technology holds great promise as a therapeutic option and a disease model.[25] However, hiPSC-CMs resemble cardiomyocytes in their embryonic stage and are immature in their phenotype, physiological stiffness, and gene expression, thus they do not fully recapitulate a functioning myocardium.[25–28] To fully utilize these highly variable cells and tissues engineered based on the hiPSC-CM technology, it is essential to be able to fully capture their architecture and compare it quantitatively among experimental groups.

In this review, we present an overview of different metrics and software for quantitative assessment of striated myocytes from images and their impact in order to facilitate future striated myocyte biology research. Additionally, we provide a look at the future of the field and the missing metrics and image analysis pipelines that could make a significant contribution to the field in the future.

II. STRIATED MYOCYTE CELLULAR MORPHOLOGY

Muscle tissue function is reliant on the specially designed organization that spans multispatial scales, all the way down to the nanoscale,[23] and connecting and choosing, which scale to focus on presents its own challenges (Fig. 1). In evaluating pathology of the heart or efficacy of stem-cell derived cells, it can be useful to measure aspects of gross cell geometry such as area, volume, and aspect ratio.[29–32] For example, in the ventricular myocardium, the cellular aspect ratio is tightly regulated (approximately 7:1),[33–35] but increases[34,35] or decreases[36,37] in some types of heart disease. Additionally, in cell culture experiments, Kuo *et al.*[32] established both a correlation between contractility and cardiomyocyte aspect ratio, as well as between cardiomyocyte aspect ratio and changes to the cytoskeletal architecture. Indeed, the cell area is an important property of the cardiomyocyte, and there are analysis pipelines that have been designed to extract it automatically from experimental images. For example, ConTraX, a pipeline that provides high throughput, morphological measurements of traction force microscopy data, enabled Pardon *et al.*[38] to evaluate

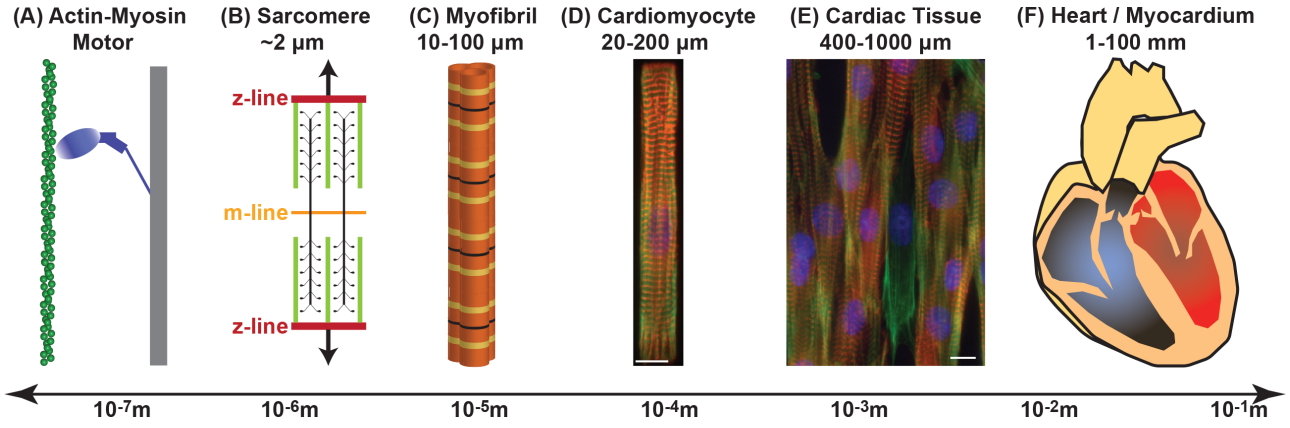

FIG. 1. A diagram of mycardium components and their relative length-scale. (a) Actin–myosin motor, (b) a sarcomere unit, (c) a myofibril composed of aligned sarcomere units, (d) a cardiomyocyte, (e) multiple cardiomyocytes in a tissue, and (f) the heart. (d) and (e) Red—α-actinin; green—actin; blue—nuclei; Scale bar: 10 μm.

the morphology of thousands of hiPSC-CMs within days as opposed to a few months.[38] In gathering quantitative data, they were able to show a significant change by day 20 of hiPSC-CMs maturation.[38] As with all automated image analysis pipelines, ConTraX requires careful handling. For instance, unintentional exclusion of certain hiPSC-CM phenotypes can occur if the morphological selection gates are not carefully defined while using ConTraX.[38] Furthermore, the throughput of ConTraX and other platforms is limited by the automation of cell differentiation and fluorescent labeling, and by the computational power of computers used.[39] While these pipelines are powerful, evaluating only cell or tissue scale architecture is insufficient to fully characterize striated muscle tissues.

III. STRIATED MYOCYTE CYTOSKELETON ARCHITECTURE

Striated myocytes are composed of parallel myofibrils that are spanned by repeating sarcomere units [Figs. 1(b)–1(e)], which are highly ordered structures that self-assemble during embryonic and post-natal development.[23,40] Organization of the striated myocyte cytoskeleton is integral to the efficiency of force production,[2,41,42] where sarcomere units produce a contractile force parallel to the thick myosin filaments as they slide past the thin actin filaments[40,43] [Fig. 2(a)]. The uniaxial force generated by muscle tissues is maximized when all sarcomeres within a cell are aligned and all cells in a tissue are aligned.[23] Consequently, myofilament disorganization has been shown to have a critical role in contractile impairment.[44,45] Furthermore, the organization of myofibrils and their sarcomeres may guide the position, shape, or organization of other organelles, in particular the mitochondria and nuclei.[46–48] Organizational guidance and changes to morphology caused by the cytoskeleton may also impact gene expression and have other downstream functional consequences.[49–52] In order to address the need to evaluate cytoskeletal architecture, many metrics and image processing tools have been developed.

A. Metrics to evaluate cytoskeleton architecture: Organization

Quantifying the organization of cytoskeletal proteins such as actin and sarcomeric α-actinin is an extremely useful tool for the characterization of striated muscle [Figs. 2(b)–2(d)]. One popular metric for measuring global construct organization, such as myofibril organization within a cell or tissue, is the orientational order parameter (OOP) [Fig. 2(b)].[2,20,53–58] The value of OOP ranges from 0 to 1 with 0 indicating complete isotropic orientation and 1 indicating perfectly aligned orientation [Fig. 2(b)].[53] The sarcomere OOP can be calculated from images [Figs. 1(d) and 1(e)] analyzed to identify constructs, such as actin and z-lines. Using the OOP to quantitatively summarize both the sarcomeric α-actinin and actin organization has shown a positive and predictive relationship between cytoskeletal alignment and contractile stresses in engineered cardiac tissues.[2,20] The OOP [Fig. 2(b)] of sarcomeric α-actinin has also been used to phenotype stem cell derived cardiomyocytes, and compare them with primary cardiomyocytes.[5,8,59] The local organization has been measured by quantifying the OOP of a construct, such as a sarcomere or actin fibril, at shorter length scales,[10] the correlation between the orientation of cellular constructs relative to other components, the co-orientational order parameter (COOP),[7] and by the sarcomere organization score developed by Sutcliffe *et al.*[29] Both experimentally and theoretically, the cytoskeletal organization has been shown to impact contraction,[2,20] underscoring the significance of quantifying this property of striated myocyte architecture. One important caveat to these metrics is that they require accurate segmentation of the construct of interest, such as a z-line, in order to accurately capture the organization of that construct. There are different ways to tackle this image analysis challenge. For example, in Morris *et al.*,[60] the local actin organization was used to isolate the α-actinin of sarcomeric z-lines from that belonging to immature stress fibrils. The proportion of α-actinin that comprised sarcomeric z-lines rather than immature stress fibers (z-line fraction) has also been used as a metric to compare engineered tissues [Fig. 2(c)].[60]

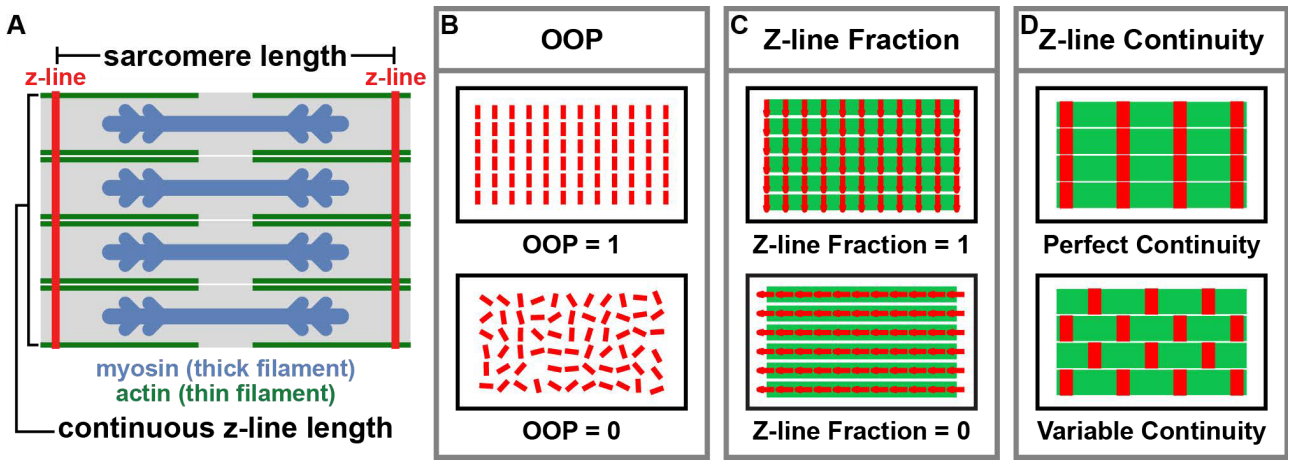

FIG. 2. Striated myocyte architectural metrics and features. (a) Schematic with a label for the sarcomere length and continuous z-line length for four myofibrils. (b) Schematic of the Orientational Order Parameter (OOP), where each red line represents a construct such as a sarcomeric z-line. (c) Schematic of the z-line fraction, where the red arrows indicate the sarcomeric z-lines and the green lines represent actin. (d) Examples of perfect continuity and variable continuity of the z-lines (red) of four parallel myofibrils (green).

To further quantify specific aspects of z-line architecture from fluorescent images and evaluate the function of engineered tissues, multiple pieces of software have been developed, such as ZlineDetection and SarcTrack (Table I).[5,18,60–62] ZlineDetection is an automated protocol that isolates z-lines and characterizes their architecture {OOP [Fig. 2(b)], Z-line fraction [Fig. 2(c)], and Z-line continuous length [Fig. 2(d)][60]} while SarcTrack is a Matlab software that can determine sarcomere content, sarcomere length [Fig. 2(a)], and rate of contractile function[61] (Table I). These analysis techniques can also be combined as demonstrated by Morris *et al.*[60] who combined SarcTrack with methods from ZlineDetection to quantify the OOP of sarcomeres and actin belonging to healthy individuals and patients with progressive heart disease.[63] The results showed that for one patient's line, the organization of sarcomeres was significantly lower than for control lines.[60]

B. Metrics to evaluate cytoskeleton architecture: Sarcomere length

Another important characteristic of striated myocytes is the sarcomere length [Fig. 2(a)],[74,75] which increases during myofibril development.[76] Accordingly, it has been commonly used to characterize the

TABLE I. Open source codes used in quantitative analyses of striated tissue.

Name	Language	Capabilities	Key measures	Link to code
ConTraX[38]	Matlab	Dynamic	Over time tracking of contractile dynamics of thousands of cells and quantifying cell area	https://github.com/MicrosystemsLab/ContraX
SarcTrack[61]	Matlab	Dynamic	Quantifying sarcomere length and content, as well as contraction and relaxation parameters	https://github.com/HMS-IDAC/SarcTrack
SOTA[29]	Matlab	Static	Cell segmentation and sarcomere registration	http://bme.virginia.edu/saucerman/[a]
Z-line detection[60]	Matlab	Static, ∼dynamic	Segmention and analysis of sarcomeric z-discs	https://github.com/Cardiovascular-Modeling-Laboratory/zlineDetection
Deepsynth[64]	ImageJ	Static	Nuclei segmentation	https://github.com/grockious/deepsynth
LoS[65]	Mathematica	Dynamic	3D fluorescent nuclei segmentation	www.physikalischebiologie.de/downloads
OpenSegSPIM[66]	Matlab	Static	Nuclei segmentation of confocal, multiphoton, and LSFM data	opensegspim.weebly.com
Other resources the reader might be interested in				
SarCoptiM[62]	ImageJ	Dynamic	Computation of spatial frequency of the striated pattern of a myocyte	https://pccv.univ-tours.fr/ImageJ/SarcOptiM/dl/SarcOptiM.zip
Sarc-Graph[59]	Python	Dynamic	Segmentation, tracking and analysis of sarcomeres	https://github.com/elejeune11/Sarc-Graph
TANGO[67]	ImageJ and R	Static	Quantitative study of nuclear organization in fluorescent images	http://biophysique.mnhn.fr/tango
MINS[68]	Matlab/C++	Static	2D and 3D segmentation of cells and nuclei detection	http://katlab-tools.org
RACE[69]	C++	Static	3D cell segmentation for confocal and LSFM data	https://bitbucket.org/jstegmaier/race/downloads/
SAMA[70]	ImageJ/R	Dynamic	Quantitative and morphological 3D analysis of cell structure	https://montevil.theobio.org/en/content/sama[a]
Vaa3D[71]	Qt/C++	Dynamic	3D visualization of gigabyte-sized microscopy images	https://github.com/Vaa3D/Vaa3D_Wiki/wiki/Download-Vaa3D-executables
3D-cell-annotator[72]	MITK	Static	3D segmentation and annotation of single cells	www.3d-cell-annotator.org
XPIWIT[73]	Qt/C++	Static	3D+t segmentation of fluorescent nuclei	https://bitbucket.org/jstegmaier/xpiwit/downloads/

[a]The link given in the paper does not work. Contact authors for a functioning link.

immaturity of stem-cell derived cardiomyocytes, which have shorter sarcomere lengths than that of primary cardiomyocytes.[5] Because measuring the sarcomere length cannot be done efficiently by hand, numerous automated software, including SarcTrack, have been developed to measure sarcomere length in images.[5,18,61,62] For example, the sarcomere content of hiPSC-CM was quantified using SarcTrack during differentiation from days 12 to 20.[61]

There are some metrics that are important characteristics of striated muscle tissue that SarcTrack is not able to extract from the images, such as continuous z-line length [Fig. 2(d)]. Due to the morphological changes of striated myocytes during development, both the sarcomere length and the continuous z-line length are essential metrics that should be included in analysis pipelines. However, depending on the pathology or maturity of the tissue, it may be necessary to measure more subtle changes in sarcomere architecture. Although SarcTrack, ZLineDetection, and other similar software offer a powerful tool to segment, track, and analyze sarcomeres, there are limitations that include a potential bias in interpreting data due to heterogeneity in sarcomere width and shape, and/or the inability to track all sarcomeres.[59]

C. Metrics to evaluate cytoskeleton architecture: Sarcomere registration and continuity

Lateral alignment of sarcomeric z-lines in neighboring myofibrils (i.e., z-line registration) has also been considered an important metric to assess striated myocytes [Fig. 2(a)].[21,32,45,77–82] Based on this prior work, it is clear that the registration has secondary importance to the overall organization of the muscle tissue. Indeed, when the sarcomeres are well organized with the same sarcomere length, it has been hypothesized that sarcomeric z-line registration influences contractile function and is an important characteristic of well-formed myofibrils.[21,32,77–82] The hypothesis has been supported by the observation of a disruption in z-line registration between adjacent myofibrils in the ventricles of failing hearts.[45] The significance of z-line registration has been investigated using both theoretical and experimental approaches,[21,32,77–81,83] which often required measuring z-line registration in images of striated muscle. Using an experimentally observable metric—the length over which z-lines of neighboring myofibrils are registered [Figs. 2(a) and 2(d)]—to approximate z-line registration, a correlation between high z-line registration and coherent, strong contractions was demonstrated in single cells.[32,79–81] However, many of these methods lack robustness, high throughput techniques, and repeatable tools to characterize z-line architecture.[60] In order to overcome the reliance on experts to manually or semi-manually measure the registration length in images, an automatic method of measuring continuous striation lengths was developed by Morris *et al.*[60] and used to quantify differences among engineered tissues. The developed computational protocol was used to (1) calculate the fraction of a z-line protein, α-actinin, that is formed into z-lines as opposed to immature stress fibrils, (2) locate the z-discs of neighboring myofibrils, and (3) measure their lengths.[60] However, a difference in striation continuity length could not fully account for functional differences between engineered isotropic and anisotropic tissues or single cells with the constant area, but variable aspect ratios.[60]

1. Additional metric: Z-line registration

In order to more successfully predict contractile stresses in engineered tissues, it may be necessary to incorporate a metric that captures the degree of z-line registration, rather than z-line continuity, into existing models of contractile function.[21] The registration parameter is a measure of the registry of alignment of z-discs across different parallel myofibrils [Fig. 2(c)]. The registry can be described as a phase-order parameter that can influence the synchronized motion of beating in a cardiomyocyte, which in turn will impact its ability to develop force.[21]

True sarcomeric registration has been calculated theoretically and for single myofibrils, manually.[21] There have been some attempts to create image processing pipelines to evaluate properties that are likely related to sarcomeric registration. For example, a pixel-based image analysis called Sarcomere Texture Analysis (SOTA)[29,84] utilizes Haralick texture features, which are defined by Haralick *et al.*[85] to be calculated from the gray level co-occurrence matrix and can be applied to any geometric shape (Table I).[85] Synthetic data of striped images that represent idealized sarcomere patterns were constructed and used to demonstrate the power of this method.[29] Each pattern produced repeated peaks in the Haralick correlation with the greatest peak magnitude corresponding to the direction of the sarcomere, which is reminiscent of the director information produced by other methods. The novelty of this method is based on measuring the decay of the Haralick Correlation as a function of offset distance, and it can extract various features of the sarcomere structure that might not be otherwise accessible.[29] However, the interpretation of these results requires more work to tie the mathematical output with variability in registration or other functional features. In the field of liquid crystal, a description of the registration of short segments is measured using the smectic order parameter.[86] In the future, it would be very interesting to develop an adaptation of the smectic order parameter from liquid crystals that could be automatically calculated for large cardiac tissues as it may be crucial in producing more accurate predictions of engineered tissue contractile function.[21]

IV. NUCLEAR MORPHOLOGY

The striated myocyte nucleus is mechanically connected to the cell membrane through the cytoskeleton, which has been shown to influence nuclear morphology.[49–52] Because changes in nuclear morphology are often accompanied by altered function, fully understanding the functional and genomic consequences of striated myocytes in pathology, aging, or in response to stimuli, requires recognizing changes to nuclear morphology.[49,52,87,88] For example, mouse models of muscle laminopathies showed nuclear envelope and DNA damage due to nuclear migration during skeletal muscle maturation that correlated with disease severity, which illustrated the importance of evaluating nuclei morphology.[89] According to Heffler *et al.*,[90] disruption in desmin, intermediate filaments that form a honeycomb-like structure that wraps around the sarcomere at the z-disk and maintains nuclear shape and the fidelity of the nuclear envelope, increases the susceptibility of cardiomyocyte nuclei to collapse, and this disruption is associated with impaired cardiomyocyte function. Thus, the nuclear shape can be an indirect measure of the proper state of cardiomyocytes and other cells.

As the characterization of nuclear morphology is an important part of many biological fields, there is an abundance of software

designed to segment nuclei in images using a large variety of image processing and deep learning approaches.[91–108] Once nuclei have been segmented, there is also a need for robust, quantitative metrics to compare and classify their morphology as normal or containing defects.[95,105] While the variability and complexity in biological phenotypes and the associated noise in signal quality make it challenging to segment the nuclei, there are multiple approaches to do so.[92] However, an important challenge is selecting the correct metrics to characterize the nuclei, including geometry as well as a relative location both of which are important to tissue function. Regarding the nuclear geometry, there is evidence of changes in size and eccentricity, as well as the presence of nuclear blebs or invaginations in pathological conditions such as cardiomyopathies and laminopathies.[109–114]

A. Additional metrics: Nuclear shape descriptors

Defining which geometric properties should be used to characterize striated myocyte nuclei, requires further investigation into the mechanisms by which their morphology impacts their function, as well as understanding these mechanisms in the context of changes to the cytoskeleton.[49,90,115] Further, expanding nuclear morphology assessment to better characterize malformations through the use of additional shape descriptors[105–107,116,117] could yield more insight into the morphological changes in cardiomyocytes from patients with disease-causing mutations. Additionally, to more fully characterize nuclear morphology, it may be beneficial to evaluate the cytoskeletal architecture surrounding each nucleus and determine the cell type or cell state to which a nucleus belongs.

V. EVALUATING ARCHITECTURAL METRICS IN THICKER TISSUES AND 3D ORGANOIDS

Traditional studies on hiPSC-CMs cultures are usually performed on a variety of culture plastic and two-dimensional (2D) substrates.[118] However, hiPSC-CMs tend to aggregate and self-assemble into a thicker tissue as opposed to forming a flat monolayer like primary cardiomyocytes,[23,63,119] which imposes challenges in imaging and analysis. While these samples are thicker, there is still a dominant planar structure, which implies that mathematically the parameters that have been described thus far in this review should still be applicable. For example, if the tissue is almost flat [Fig. 3(a)], it is best to calculate the OOP [Fig. 2(b)] in the horizontal plane using the standard equations normally utilized for 2D constructs, such as actin myofibrils[63] [Eq. (1)]. The OOP in 2D can be calculated using:

$$OOP_{2D} = \langle \cos(2\theta) \rangle = \langle 2\cos^2(\theta) - 1 \rangle, \quad (1)$$

where θ is the angle between each construct and the director, i.e., main direction of all constructs. However, to accurately apply the parameters, the pipelines of imaging and feature extraction need to be appropriately adjusted for each feature and parameter of interest. Imaging somewhat thick specimens is possible using confocal microscopy and optical sectioning [Figs. 3(b)–3(d)].[63]

In the long run, moving from cell monolayers to true three-dimensional (3D) cultures is one of the pathways that is being pursued to more accurately mimic the function of living tissues.[23] Subsequently, the need for dynamic quantitative analysis of 3D biological structures with excellent optical sectioning capability is an emerging necessity.[120] Furthermore, as such imaging becomes realistic, it will be necessary to adjust the suite of architectural parameters to true 3D representation.

A. Thicker tissue: Nuclei

Automated segmentation of confocal images is challenging because characteristics that are obvious to the human eye are frequently difficult to translate into quantitative results that can be used by a computer. One challenge in analyzing thicker tissues is separating individual DAPI stained nuclei that appeared in multiple z-slices [Fig. 3(a)]. This can be achieved by using Deepsynth, a modified version of a 3D convolutional neural network that uses machine-learning techniques,[64] the 3D Iterative Thresholding (IT), an algorithm impeded in 3D ImageJ Suite of ImageJ/Fiji,[121] Lines-of-Sight (LoS), an automated method to segment 3D fluorescent images,[65] or OpenSegSPIM, a 3D automatic quantitative analysis tool for confocal data (Table I).[66] Nuclear segmentation can also be performed in several steps that break the images apart for analysis that can be achieved with prior pipelines.[95] First, each z-slice needs to be segmented and nuclei should be grouped after comparing the segmentation results for each neighboring z-slice, such that continuity is maintained for each nucleus. Then, the maximum projection of each single nucleus can be separately saved after verification from the user [Fig. 3(b)].[63] As long as one of these methods successfully isolates and concatenates each nucleus from each z-slice where it exists, the nuclei can be analyzed for

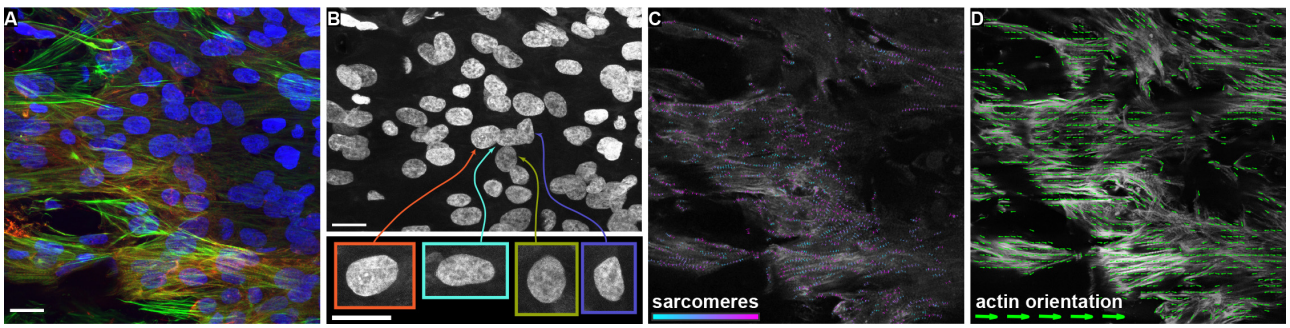

FIG. 3. Analysis of thicker tissues engineered from iPSC-derived cardiomyocytes. (a) Merge maximum projection of a confocal stack showing DAPI, green—actin, red—α-actinin. (b) DAPI stain showing multiple overlaid nuclei with segmentation results. (c) One confocal slice with sarcomere detection results. (d) One confocal slice with actin orientation detection. Scale bar: 20 μm.

their morphological properties even if in a classical maximum projection image, the nuclei overlap. The power of such methods is that they reduce the imaging pipeline for use with any previous method and can be applied to many organelles that span multiple optical slices.

B. Thicker tissue: Sarcomeres

For some structures, the imaging is not yet at a level where it is possible to reconstruct the 3D organelle. For example, sarcomeres, even in 2D, are analyzed pixel by pixel. Thus, a completely different approach can be taken when working with analyzing sarcomere architecture in thicker tissues. Namely, the sarcomere structure can be reconstructed using confocal microscopy and optical sectioning. After sectioning the tissue into slices, each slice's sarcomeres can then be analyzed using developed algorithms such as SarcTrack (Sec. III B),[61] Sarcomere Texture Analysis (SOTA),[29,84] and ZlineDetection.[60] Even though each algorithm is theoretically capable of assessing sarcomeres on its own, the current state-of-the-art method is to combine a few of these algorithms because hiPSC-CMs often lack striations, the characteristics of mature cardiac myocytes,[23] which makes the images extremely noisy for analysis. As a result of the hiPSC-CMs sarcomeres immaturity and non-linearity[23] [Figs. 3(a) and 3(c)], the shear amount of inherent noise overwhelms any of the existing image processing pipelines if used alone.

To take full advantage of the filtering capability of the ZlineDetection method,[60] it is also necessary to reconstruct the actin architecture in a thicker sample, and couple it with the sarcomere location and orientation. If the orientation of actin in thicker tissues is calculated, the distribution can be visualized by plotting the angle frequency as a function of its distribution Han *et al.*[122] Alternatively, the orientation of actin in thicker tissue can be evaluated with many existing metrics such as the 3D directional variance algorithm, which is based on the extension of a previously established 2D weighted vector summation technique Liu *et al.*[123] or the curvelet-based alignment analysis software where the orientation can be quantified by measuring its angle relative to the axis direction. Another method to measure the orientation in each 3D slice is by first enhancing the contrast of each actin stained optical slice. Second, each image is filtered with a Gaussian kernel and normalized from which the orientation vectors can be calculated. Third, the orientation vectors for each optical slice are concatenated for the field of view and then for the entire sample. The information on actin orientation can be useful on its own, by calculating the orientation order of actin in the sample [Eq. (1)][63] of all of the vectors in the whole volume of the tissue [Fig. 3(d)]. Alternatively, the detailed information on actin directions for each optical slice can be used to eliminate some of the noise inherent in the ZlineDetection pipe-lines when applied to highly noisy images[63] [Fig. 3(c)]. Once these constructs, i.e., z-lines, sarcomere edges, or actin, have been identified the OOP for any of these [Fig. 2(b)] can be calculated for each experimental condition.[63]

C. 3D organoids

Because the actin cytoskeleton ensures the structural and mechanical integrity of cells[124] and is essential to the mechanosensitivity and mechanical response of adhering cells to their environment,[125–128] it may be important to characterize 3D actin organization in true 3D organoids. Other constructs, such as z-lines and extracellular matrix might also be important to evaluate in true 3D organoids.

While this has not yet been tackled, it is possible to adapt existing algorithms to output a 3D vector for each construct pixel. Then, construct organization in 3D could be measured by computing a 3D orientation vector for each pixel, and using the 3D nematic order parameter (3D OOP) to quantify the organization, which can be calculated using[129]

$$OOP_{3D} = \left\langle \frac{3\cos^2(\theta) - 1}{2} \right\rangle, \tag{2}$$

where θ is the angle between the construct of interest and the "average" direction, i.e., director.

VI. MUSCLE TISSUE WITH MULTIPLE CELL-TYPES

Studying interactions between morphologically or phenotypically distinct cells is a vital aspect of understanding biological processes,[130] such as the role of smooth and skeletal muscle in esophageal function,[131] the cardiac remodeling response of cardiomyocytes and cardiac fibroblasts [Figs. 4(a)–4(c)],[132–134] and the variability in the cell types and functionality produced from cardiac differentiation from induced pluripotent stem cells.[8,29,135] Therefore, in order to study interactions or differences between morphologically distinct cells, it is necessary to accurately and reliably separate them in images, which can be extremely challenging to do by hand in a high-throughput manner, particularly in confluent tissues. To combat this issue, image-based cell profiling commonly makes use of machine learning

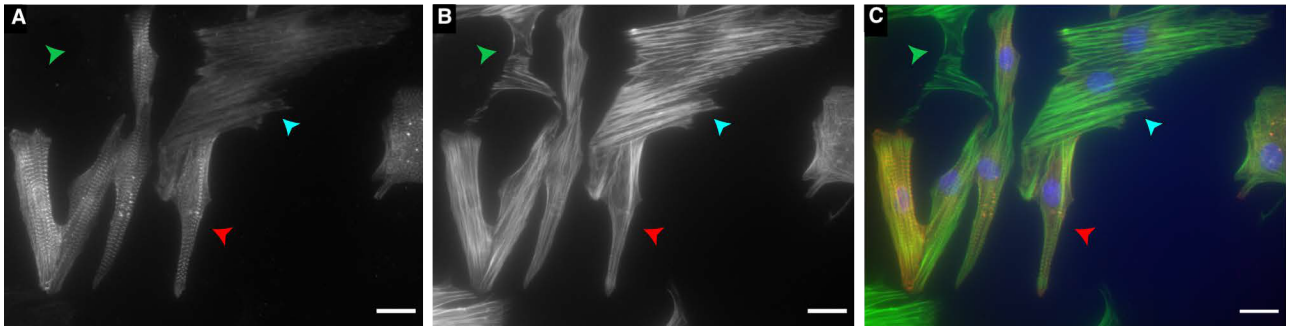

FIG. 4. Images of neonatal rat cardiomyocytes and fibroblasts stained for (a) α-actinin [(c), red], (b) actin [(c), green], and DAPI [(c), blue]. The arrowheads in (a)–(c) point to a fibroblast (green), a cardiomyocyte (red), and a cell with no identifiable sarcomere striations (cyan). Scale bars: 20 μm.

classifiers and feature extraction, as well as deep learning approaches.[67,85,101,103,130,136–142] Once the cell type or cell state segmentation has been achieved, it can be combined with other analysis to unlock even more biological information, including studying interactions between different cells.[31] However, it is extremely difficult to create a classifier that can correctly account for the large spread of biological and experimental variability, especially while considering the unique morphology of striated myocytes, which makes this the next challenge in the field.

VII. ANALYSIS OF DYNAMIC DATA

Striated muscle is inherently dynamic during the contraction process, and the dynamic deformations result in rhythmically evolving cytoskeleton architecture and nuclei geometry. With the advent of multi-photon microscopy, stem-cell derived muscle that can be fluorescently tagged for specific constructs such as z-lines, and fast cameras, it is now possible to collect serial images, i.e., movies, of muscle cytoskeleton and organelles. Therefore, image analysis pipelines that are capable of tracking the cellular features dynamically[38,39,59,61] are important to the future of the field (indicated in Table I). The first step in converting static analysis to analyze dynamic data are to automate the analysis of each image in the movie, which can be easily applied to many of the static codes in Table I. For example, Z-Line detection[60] can be easily looped to analyze previously published data[61] of beating sarcomeres. However, true dynamical analysis also requires continuous tracking of the structures of interest during the movement. While this presents an added challenge, the future benefits to the field are essential as for example, dynamics of sarcomeres[61] can be directly tied to function such as local strains and developed force directions.

VIII. FUTURE DIRECTIONS

Biological 3D image stacks contain rich data that require well-developed, automated digital analysis methods. Using machine learning approaches is efficient when a specific repetitive task or classification is needed if an appropriated training set can be created. For example, machine learning has already been applied to the task of nuclei segmentation. In the study of Dunn *et al.*,[64] the tedious process of manually training the algorithm to outline individual nuclei was performed successfully. Challenges that still remain are, for example, creating training datasets of cell boundary to develop algorithms to automate the process. Another such challenge is in analyzing heterogeneous cell architecture, such as sarcomeres because, it is incredibly hard to define a large enough training set manually. The techniques and metrics in this review might be the future if they are coupled with machine learning algorithms. This is especially true if the analysis of the data gathered by the algorithms is coupled with machine learning techniques, which has been done with some structural aspects of cardiomyocytes.[8] Still, if machine learning algorithms can be trained to detect cell border or individual sarcomeres, a lot of data can be extracted from 3D biological image stacks and high throughput data, which will enrich both the classical and machine learning analysis of healthy vs pathological tissues.

IX. CONCLUSION

Here, we presented an overview of image processing and analysis techniques for the assessment of striated myocytes. The unique nature of these cells necessitates the use of advanced image analysis techniques. While there have been many advances in computer vision and biological image analysis,[143] many tools are not applicable for characterizing striated myocytes' architecture without further modification. The specialized pipelines designed for striated myocytes have yielded great insight into the structure–function relationship and architectural changes during pathology. As this review demonstrates, widespread adaptation and additional development of these computational techniques will enable further advances in the field of striated myocyte morphology.

ACKNOWLEDGMENTS

This work was supported by the Edwards Lifesciences Center for Advanced Cardiovascular Technology's Training Grant Nos. NIH T32 HL116270 (PI: Hughes, Trainee: TAM), NIH R01 HL129008 (MPI: Grosberg, Zaragoza), NIH R03 EB028605 (PI: Grosberg), NSF DMS1763272 (PI: Nie), and a grant from the Simons Foundation Grant No. 594598 (PI: Nie).

AUTHOR DECLARATIONS

Conflict of Interest

The authors have no conflicts to disclose.

Author Contributions

Tessa Altair Morris: Conceptualization (equal); Writing – original draft (equal). **Sarah Eldeen:** Writing – original draft (supporting); Writing – review & editing (lead). **Richard Duc Hien Tran:** Writing – original draft (supporting). **Anna Grosberg:** Conceptualization (equal); Writing – original draft (equal); Writing – review & editing (equal).

DATA AVAILABILITY

Data sharing is not applicable to this article as no new data were created or analyzed in this article.

REFERENCES

[1]J. A. Rall, "What makes skeletal muscle striated? Discoveries in the endosarcomeric and exosarcomeric cytoskeleton," Adv. Physiol. Educ. **42**, 672–684 (2018).
[2]M. B. Knight, N. K. Drew, L. A. McCarthy, and A. Grosberg, "Emergent global contractile force in cardiac tissues," Biophys. J. **110**, 1615–1624 (2016).
[3]E. Ehler, B. Rothen, S. Hammerle, M. Komiyama, and J. Perriard, "Myofibrillogenesis in the developing chicken heart: Assembly of z-disk, m-line and the thick filaments," J. Cell Sci. **112**, 1529–1539 (1999).
[4]J. W. Sanger, J. C. Ayoob, P. Chowrashi, D. Zurawski, and J. M. Sanger, "Assembly of myofibrils in cardiac muscle cells," in *Elastic Filaments of the Cell* (Springer, 2000), pp. 89–110.
[5]S. P. Sheehy, F. Pasqualini, A. Grosberg, S. J. Park, Y. Aratyn-Schaus, and K. K. Parker, "Quality metrics for stem cell-derived cardiac myocytes," Stem Cell Rep. **2**, 282–294 (2014).
[6]L. M. Larkin, S. Calve, T. Y. Kostrominova, and E. M. Arruda, "Structure and functional evaluation of tendon–skeletal muscle constructs engineered *in vitro*," Tissue Eng. **12**, 3149–3158 (2006).
[7]N. K. Drew, M. A. Eagleson, D. B. Baldo, Jr., K. K. Parker, and A. Grosberg, "Metrics for assessing cytoskeletal orientational correlations and consistency," PLoS Comput. Biol. **11**, e1004190 (2015).
[8]F. S. Pasqualini, S. P. Sheehy, A. Agarwal, Y. Aratyn-Schaus, and K. K. Parker, "Structural phenotyping of stem cell-derived cardiomyocytes," Stem Cell Rep. **4**, 340–347 (2015).

[9]A. J. Ribeiro, Y.-S. Ang, J.-D. Fu, R. N. Rivas, T. M. Mohamed, G. C. Higgs, D. Srivastava, and B. L. Pruitt, "Contractility of single cardiomyocytes differentiated from pluripotent stem cells depends on physiological shape and substrate stiffness," Proc. Natl. Acad. Sci. U. S. A. **112**, 12705–12710 (2015).
[10]N. K. Drew, N. E. Johnsen, J. Q. Core, and A. Grosberg, "Multiscale characterization of engineered cardiac tissue architecture," J. Biomech. Eng. **138**, 111003 (2016).
[11]J. Schaper, R. Froede, A. Buck, and N. Bleese, "Impaired myocardial ultrastructure and cytoskeleton in cardiomyopathic human myocardium," in *New Concepts in Viral Heart Disease* (Springer, 1988), pp. 295–302.
[12]G. M. Conover, S. N. Henderson, and C. C. Gregorio, "A myopathy-linked desmin mutation perturbs striated muscle actin filament architecture," Mol. Biol. Cell **20**, 834–845 (2009).
[13]A. Gupta, S. Gupta, D. Young, B. Das, J. McMahon, and S. Sen, "Impairment of ultrastructure and cytoskeleton during progression of cardiac hypertrophy to heart failure," Lab. Invest. **90**, 520 (2010).
[14]G. Wang, M. L. McCain, L. Yang, A. He, F. S. Pasqualini, A. Agarwal, H. Yuan, D. Jiang, D. Zhang, L. Zangi *et al.*, "Modeling the mitochondrial cardiomyopathy of Barth syndrome with induced pluripotent stem cell and heart-on-chip technologies," Nat. Med. **20**, 616 (2014).
[15]R. Armstrong, R. Ogilvie, and J. Schwane, "Eccentric exercise-induced injury to rat skeletal muscle," J. Appl. Physiol. **54**, 80–93 (1983).
[16]J. Friden, M. Sjöström, and B. Ekblom, "Myofibrillar damage following intense eccentric exercise in man," Int. J. Sports Med. **4**, 170–176 (1983).
[17]S. Wood, D. Morgan, and U. Proske, "Effects of repeated eccentric contractions on structure and mechanical properties of toad sartorius muscle," Am. J. Physiol. **265**, C792–C800 (1993).
[18]C. Balnave, D. Davey, and D. Allen, "Distribution of sarcomere length and intracellular calcium in mouse skeletal muscle following stretch-induced injury," J. Physiol. **502**, 649–659 (1997).
[19]K. R. Doherty, D. R. Talbert, P. B. Trusk, D. M. Moran, S. A. Shell, and S. Bacus, "Structural and functional screening in human induced-pluripotent stem cell-derived cardiomyocytes accurately identifies cardiotoxicity of multiple drug types," Toxicol. Appl. Pharmacol. **285**, 51–60 (2015).
[20]A. W. Feinberg, P. W. Alford, H. Jin, C. M. Ripplinger, A. A. Werdich, S. P. Sheehy, A. Grosberg, and K. K. Parker, "Controlling the contractile strength of engineered cardiac muscle by hierarchal tissue architecture," Biomaterials **33**, 5732–5741 (2012).
[21]K. Dasbiswas, S. Majkut, D. Discher, and S. A. Safran, "Substrate stiffness-modulated registry phase correlations in cardiomyocytes map structural order to coherent beating," Nat. Commun. **6**, 6085 (2015).
[22]K. A. Clark, A. S. McElhinny, M. C. Beckerle, and C. C. Gregorio, "Striated muscle cytoarchitecture: An intricate web of form and function," Annu. Rev. Cell Dev. Biol. **18**, 637–706 (2002).
[23]M. B. Knight, A. Grosberg, and M. L. McCain, "*In vitro* tools for quantifying structure–function relationships in cardiac myocyte cells and tissues," in *Cardiac Cytoarchitecture* (Springer, 2015), pp. 15–39.
[24]P. Ahuja, P. Sdek, and W. R. MacLellan, "Cardiac myocyte cell cycle control in development, disease, and regeneration," Physiol. Rev. **87**, 521–544 (2007).
[25]B. L. Tang, "Maturing iPSC-derived cardiomyocytes," Cells **9**, 213 (2020).
[26]Y. Guo and W. T. Pu, "Cardiomyocyte maturation," Circ. Res. **126**, 1086–1106 (2020).
[27]H. S. Hwang, D. O. Kryshtal, T. Feaster, V. Sánchez-Freire, J. Zhang, T. J. Kamp, C. C. Hong, J. C. Wu, and B. C. Knollmann, "Comparable calcium handling of human iPSC-derived cardiomyocytes generated by multiple laboratories," J. Mol. Cell. Cardiol. **85**, 79–88 (2015).
[28]F. S. Pasqualini, A. Agarwal, B. B. O'Connor, Q. Liu, S. P. Sheehy, and K. K. Parker, "Traction force microscopy of engineered cardiac tissues," PLoS One **13**, e0194706 (2018).
[29]M. D. Sutcliffe, P. M. Tan, A. Fernandez-Perez, Y.-J. Nam, N. V. Munshi, and J. J. Saucerman, "High content analysis identifies unique morphological features of reprogrammed cardiomyocytes," Sci. Rep. **8**, 1258 (2018).
[30]J. G. Bensley, R. De Matteo, R. Harding, and M. J. Black, "Three-dimensional direct measurement of cardiomyocyte volume, nuclearity, and ploidy in thick histological sections," Sci. Rep. **6**, 23756 (2016).
[31]A. Oliver-Gelabert, L. García-Mendívil, J. M. Vallejo-Gil, P. C. Fresneda-Roldán, K. Andelová, J. Fañanás-Mastral, M. Vázquez-Sancho, M. Matamala-Adell, F. Sorribas-Berjón, C. Ballester-Cuenca *et al.*, "Automatic quantification of cardiomyocyte dimensions and connexin 43 lateralization in fluorescence images," Biomolecules **10**, 1334 (2020).
[32]P.-L. Kuo, H. Lee, M.-A. Bray, N. A. Geisse, Y.-T. Huang, W. J. Adams, S. P. Sheehy, and K. K. Parker, "Myocyte shape regulates lateral registry of sarcomeres and contractility," Am. J. Pathol. **181**, 2030–2037 (2012).
[33]A. M. Gerdes, "Cardiac myocyte remodeling in hypertrophy and progression to failure," J. Card. Failure **8**, S264–S268 (2002).
[34]A. M. Gerdes and J. M. Capasso, "Structural remodeling and mechanical dysfunction of cardiac myocytes in heart failure," J. Mol. Cell. Cardiol. **27**, 849–856 (1995).
[35]A. M. Gerdes, S. E. Kellerman, J. A. Moore, K. E. Muffly, L. C. Clark, P. Y. Reaves, K. B. Malec, P. P. McKeown, and D. D. Schocken, "Structural remodeling of cardiac myocytes in patients with ischemic cardiomyopathy," Circulation **86**, 426–430 (1992).
[36]Z. A. McCrossan, R. Billeter, and E. White, "Transmural changes in size, contractile and electrical properties of SHR left ventricular myocytes during compensated hypertrophy," Cardiovasc. Res. **63**, 283–292 (2004).
[37]K-i Sawada and K. Kawamura, "Architecture of myocardial cells in human cardiac ventricles with concentric and eccentric hypertrophy as demonstrated by quantitative scanning electron microscopy," Heart Vessels **6**, 129–142 (1991).
[38]G. Pardon, H. Lewis, A. S. V. Roest, E. A. Castillo, R. Wilson, A. K. Denisin, C. A. Blair, F. Birnbaum, C. Holbrook, K. Koleckar, A. C.-Y. Chang, H. M. Blau, and B. L. Pruitt, "Insights into single hiPSC-derived cardiomyocyte phenotypes and maturation using ConTraX, an efficient pipeline for tracking contractile dynamics," bioRxiv:2021.03.18.436014 (2021).
[39]A. J. Ribeiro, O. Schwab, M. A. Mandegar, Y.-S. Ang, B. R. Conklin, D. Srivastava, and B. L. Pruitt, "Multi-imaging method to assay the contractile mechanical output of micropatterned human iPSC-derived cardiac myocytes," Circ. Res. **120**, 1572–1583 (2017).
[40]J. W. Sanger, J. Wang, Y. Fan, J. White, and J. M. Sanger, "Assembly and dynamics of myofibrils," BioMed Res. Int. **2010**, 858606.
[41]J. Robbins, "Diseases of the cytoskeleton: The desminopathies," in *Cardioskeletal Myopathies Children Young Adults* (Academic Press, 2017), pp. 173–192.
[42]M. Stromer, "The cytoskeleton in skeletal, cardiac and smooth muscle cells," Histol. Histopathol. **13**, 283 (1998).
[43]A. Grosberg, P.-L. Kuo, C.-L. Guo, N. A. Geisse, M.-A. Bray, W. J. Adams, S. P. Sheehy, and K. K. Parker, "Self-organization of muscle cell structure and function," PLoS Comput. Biol. **7**, e1001088 (2011).
[44]N. G. Pérez, K. Hashimoto, S. McCune, R. A. Altschuld, and E. Marbán, "Origin of contractile dysfunction in heart failure: Calcium cycling versus myofilaments," Circulation **99**, 1077–1083 (1999).
[45]J. Schaper, R. Froede, S. Hein, A. Buck, H. Hashizume, B. Speiser, A. Friedl, and N. Bleese, "Impairment of the myocardial ultrastructure and changes of the cytoskeleton in dilated cardiomyopathy," Circulation **83**, 504–514 (1991).
[46]G. Benard, B. Faustin, E. Passerieux, A. Galinier, C. Rocher, N. Bellance, J.-P. Delage, L. Casteilla, T. Letellier, and R. Rossignol, "Physiological diversity of mitochondrial oxidative phosphorylation," Am. J. Physiol. **291**, C1172–C1182 (2006).
[47]N. M. Ramdas and G. Shivashankar, "Cytoskeletal control of nuclear morphology and chromatin organization," J. Mol. Biol. **427**, 695–706 (2015).
[48]F. Li, X. Wang, and A. M. Gerdes, "Formation of binucleated cardiac myocytes in rat heart. II. cytoskeletal organisation," J. Mol. Cell. Cardiol. **29**, 1553–1565 (1997).
[49]M.-A. P. Bray, W. J. Adams, N. A. Geisse, A. W. Feinberg, S. P. Sheehy, and K. K. Parker, "Nuclear morphology and deformation in engineered cardiac myocytes and tissues," Biomaterials **31**, 5143–5150 (2010).
[50]J. Lammerding, "Mechanics of the nucleus," Compr. Physiol. **1**, 783–807 (2011).
[51]R. Vishavkarma, S. Raghavan, C. Kuyyamudi, A. Majumder, J. Dhawan, and P. A. Pullarkat, "Role of actin filaments in correlating nuclear shape and cell spreading," PLoS One **9**, e107895 (2014).

[52]N. Jain, K. V. Iyer, A. Kumar, and G. Shivashankar, "Cell geometric constraints induce modular gene-expression patterns via redistribution of hdac3 regulated by actomyosin contractility," Proc. Natl. Acad. Sci. U. S. A. **110**, 11349–11354 (2013).
[53]A. Grosberg, P. W. Alford, M. L. McCain, and K. K. Parker, "Ensembles of engineered cardiac tissues for physiological and pharmacological study: Heart on a chip," Lab Chip **11**, 4165–4173 (2011).
[54]J. Sun, J. Tang, and J. Ding, "Cell orientation on a stripe-micropatterned surface," Chin. Sci. Bull. **54**, 3154–3159 (2009).
[55]A. Umeno and S. Ueno, "Quantitative analysis of adherent cell orientation influenced by strong magnetic fields," IEEE Trans. Nanobiosci. **2**, 26–28 (2003).
[56]D. Volfson, S. Cookson, J. Hasty, and L. S. Tsimring, "Biomechanical ordering of dense cell populations," Proc. Natl. Acad. Sci. U. S. A **105**, 15346–15351 (2008).
[57]I. W. Hamley, *Introduction to Soft Matter: Synthetic and Biological Self-Assembling Materials* (John Wiley and Sons, 2013).
[58]Q. Hu, T. A. Morris, A. Grosberg, A. J. Levine, and E. L. Botvinick, "Actively driven fluctuations in a fibrin network," Front. Phys. **8**, 568736 (2021).
[59]B. Zhao, K. Zhang, C. S. Chen, and E. Lejeune, "Sarc-Graph: Automated segmentation, tracking, and analysis of sarcomeres in hiPSC-derived cardiomyocytes," PLOS Comput. Biol. **17**, e1009443 (2021).
[60]T. A. Morris, J. Naik, K. S. Fibben, X. Kong, T. Kiyono, K. Yokomori, and A. Grosberg, "Striated myocyte structural integrity: Automated analysis of sarcomeric z-discs," PLoS Comput. Biol. **16**, e1007676 (2020).
[61]C. N. Toepfer, A. Sharma, M. Cicconet, A. C. Garfinkel, M. Mücke, M. Neyazi, J. A. Willcox, R. Agarwal, M. Schmid, J. Rao *et al.*, "SarcTrack: An adaptable software tool for efficient large-scale analysis of sarcomere function in hiPSC-cardiomyocytes," Circ. Res. **124**, 1172–1183 (2019).
[62]C. Pasqualin, F. Gannier, A. Yu, C. O. Malécot, P. Bredeloux, and V. Maupoil, "SarcOptiM for ImageJ: High-frequency online sarcomere length computing on stimulated cardiomyocytes," Am. J. Physiol. **311**, C277–C283 (2016).
[63]M. Mehrabi, T. A. Morris, Z. Cang, C. H. H. Nguyen, Y. Sha, M. N. Asad, N. Khachikyan, T. L. Greene, D. M. Becker, Q. Nie, M. V. Zaragoza, and A. Grosberg, "A study of gene expression, structure, and contractility of iPSC-derived cardiac myocytes from a family with heart disease due to LMNA mutation," Ann. Biomed. Eng. **49**, 3524 (2021).
[64]K. W. Dunn, C. Fu, D. J. Ho, S. Lee, S. Han, P. Salama, and E. J. Delp, "DeepSynth: Three-dimensional nuclear segmentation of biological images using neural networks trained with synthetic data," Sci. Rep. **9**, 18295 (2019).
[65]B. Mathew, A. Schmitz, S. Muñoz-Descalzo, N. Ansari, F. Pampaloni, E. Stelzer, and S. Fischer, "Robust and automated three-dimensional segmentation of densely packed cell nuclei in different biological specimens with lines-of-sight decomposition," BMC Bioinf. **16**, 187 (2015).
[66]L. Gole, K. H. Ong, T. Boudier, W. Yu, and S. Ahmed, "OpenSegSPIM: A user-friendly segmentation tool for SPIM data," Bioinformatics **32**, 2075–2077 (2016).
[67]J. Ollion, J. Cochennec, F. Loll, C. Escudé, and T. Boudier, "TANGO: A generic tool for high-throughput 3D image analysis for studying nuclear organization," Bioinformatics **29**, 1840–1841 (2013).
[68]X. Lou, M. Kang, P. Xenopoulos, S. Muñoz-Descalzo, and A.-K. Hadjantonakis, "A rapid and efficient 2D/3D nuclear segmentation method for analysis of early mouse embryo and stem cell image data," Stem Cell Rep. **2**, 382–397 (2014).
[69]J. Stegmaier, F. Amat, W. C. Lemon, K. McDole, Y. Wan, G. Teodoro, R. Mikut, and P. J. Keller, "Real-time three-dimensional cell segmentation in large-scale microscopy data of developing embryos," Dev. Cell **36**, 225–240 (2016).
[70]T. Paulose, M. Montévil, L. Speroni, F. Cerruti, C. Sonnenschein, and A. M. Soto, "SAMA: A method for 3D morphological analysis," PLoS One **11**, e0153022 (2016).
[71]H. Peng, Z. Ruan, F. Long, J. H. Simpson, and E. W. Myers, "V3D enables real-time 3D visualization and quantitative analysis of large-scale biological image data sets," Nat. Biotechnol. **28**, 348–353 (2010).
[72]E. A. Tasnadi, T. Toth, M. Kovacs, A. Diosdi, F. Pampaloni, J. Molnar, F. Piccinini, and P. Horvath, "3D-cell-annotator: An open-source active surface tool for single-cell segmentation in 3D microscopy images," Bioinformatics **36**, 2948–2949 (2020).
[73]A. Bartschat, E. Hübner, M. Reischl, R. Mikut, and J. Stegmaier, "XPIWIT—an XML pipeline wrapper for the insight toolkit," Bioinformatics **32**, 315 (2015).
[74]P. P. de Tombe and H. E. ter Keurs, "Cardiac muscle mechanics: Sarcomere length matters," J. Mol. Cell. Cardiol. **91**, 148–150 (2016).
[75]D. A. Pavlov and A. Landesberg, "The cross-bridge dynamics is determined by two length-independent kinetics: Implications on muscle economy and Frank–Starling law," J. Mol. Cell. Cardiol. **90**, 94–101 (2016).
[76]J. W. Sanger, J. Wang, B. Holloway, A. Du, and J. M. Sanger, "Myofibrillogenesis in skeletal muscle cells in zebrafish," Cell Motil. Cytoskeleton **66**, 556–566 (2009).
[77]K. S. Campbell, "Interactions between connected half-sarcomeres produce emergent mechanical behavior in a mathematical model of muscle," PLoS Comput. Biol. **5**, e1000560 (2009).
[78]B. M. Friedrich, A. Buxboim, D. E. Discher, and S. A. Safran, "Striated actomyosin fibers can reorganize and register in response to elastic interactions with the matrix," Biophys. J. **100**, 2706–2715 (2011).
[79]A. G. Rodriguez, S. J. Han, M. Regnier, and N. J. Sniadecki, "Substrate stiffness increases twitch power of neonatal cardiomyocytes in correlation with changes in myofibril structure and intracellular calcium," Biophys. J. **101**, 2455–2464 (2011).
[80]S. Majkut, T. Idema, J. Swift, C. Krieger, A. Liu, and D. E. Discher, "Heart-specific stiffening in early embryos parallels matrix and myosin expression to optimize beating," Curr. Biol. **23**, 2434–2439 (2013).
[81]N. Hersch, B. Wolters, G. Dreissen, R. Springer, N. Kirchgeßner, R. Merkel, and B. Hoffmann, "The constant beat: Cardiomyocytes adapt their forces by equal contraction upon environmental stiffening," Biol. Open **2**, 351–361 (2013).
[82]K. Dasbiswas, S. Hu, F. Schnorrer, S. A. Safran, and A. D. Bershadsky, "Ordering of myosin II filaments driven by mechanical forces: Experiments and theory," Philos. Trans. R. Soc., B **373**, 20170114 (2018).
[83]M. Sam, S. Shah, J. Fridén, D. J. Milner, Y. Capetanaki, and R. L. Lieber, "Desmin knockout muscles generate lower stress and are less vulnerable to injury compared with wild-type muscles," Am. J. Physiol. **279**, C1116–C1122 (2000).
[84]R. M. Haralick, "Statistical and structural approaches to texture," Proc. IEEE **67**, 786–804 (1979).
[85]R. M. Haralick, K. Shanmugam, and I. H. Dinstein, "Textural features for image classification," IEEE Trans. Syst., Man, Cybern. **3**, 610–621 (1973).
[86]W. L. McMillan, "Simple molecular model for the Smectic *A* phase of liquid crystals," Phys. Rev. A **4**, 1238–1246 (1971).
[87]K. Tokunaga, N. Saitoh, I. G. Goldberg, C. Sakamoto, Y. Yasuda, Y. Yoshida, S. Yamanaka, and M. Nakao, "Computational image analysis of colony and nuclear morphology to evaluate human induced pluripotent stem cells," Sci. Rep. **4**, 6996 (2014).
[88]P. Scaffidi and T. Misteli, "Lamin A-dependent nuclear defects in human aging," Science **312**, 1059–1063 (2006).
[89]A. J. Earle, T. J. Kirby, G. R. Fedorchak, P. Isermann, J. Patel, S. Iruvanti, S. A. Moore, G. Bonne, L. L. Wallrath, and J. Lammerding, "Mutant lamins cause nuclear envelope rupture and DNA damage in skeletal muscle cells," Nat. Mater. **19**, 464–473 (2020).
[90]J. Heffler, P. P. Shah, P. Robison, S. Phyo, K. Veliz, K. Uchida, A. Bogush, J. Rhoades, R. Jain, and B. L. Prosser, "A balance between intermediate filaments and microtubules maintains nuclear architecture in the cardiomyocyte," Circ. Res. **126**, e10–e26 (2020).
[91]F. Xing and L. Yang, "Robust nucleus/cell detection and segmentation in digital pathology and microscopy images: A comprehensive review," IEEE Rev. Biomed. Eng. **9**, 234–263 (2016).
[92]J. C. Caicedo, J. Roth, A. Goodman, T. Becker, K. W. Karhohs, M. Broisin, C. Molnar, C. McQuin, S. Singh, F. J. Theis *et al.*, "Evaluation of deep learning strategies for nucleus segmentation in fluorescence images," Cytometry, Part A **95**, 952–965 (2019).
[93]J. C. Caicedo, A. Goodman, K. W. Karhohs, B. A. Cimini, J. Ackerman, M. Haghighi, C. Heng, T. Becker, M. Doan, C. McQuin *et al.*, "Nucleus

segmentation across imaging experiments: The 2018 data science bowl," Nat. Methods **16**, 1247–1253 (2019).
[94]M. Salvi, U. Morbiducci, F. Amadeo, R. Santoro, F. Angelini, I. Chimenti, D. Massai, E. Messina, A. Giacomello, M. Pesce *et al.*, "Automated segmentation of fluorescence microscopy images for 3D cell detection in human-derived cardiospheres," Sci. Rep. **9**, 6644 (2019).
[95]J. Q. Core, M. Mehrabi, Z. R. Robinson, A. R. Ochs, L. A. McCarthy, M. V. Zaragoza, and A. Grosberg, "Age of heart disease presentation and dysmorphic nuclei in patients with LMNA mutations," PloS One **12**, e0188256 (2017).
[96]O. Boonsiri, K. Washiya, K. Aoki, and H. Nagahashi, "3D gray level co-occurrence matrix based classification of favor benign and borderline types in follicular neoplasm images," J. Biosci. Med. **4**, 51 (2016).
[97]A. Gertych, Z. Ma, J. Tajbakhsh, A. Velásquez-Vacca, and B. S. Knudsen, "Rapid 3D delineation of cell nuclei for high-content screening platforms," Comput. Biol. Med. **69**, 328–338 (2016).
[98]G. Lin, U. Adiga, K. Olson, J. F. Guzowski, C. A. Barnes, and B. Roysam, "A hybrid 3D watershed algorithm incorporating gradient cues and object models for automatic segmentation of nuclei in confocal image stacks," Cytometry, Part A **56**, 23–36 (2003).
[99]G. Li, T. Liu, A. Tarokh, J. Nie, L. Guo, A. Mara, S. Holley, and S. T. Wong, "3D cell nuclei segmentation based on gradient flow tracking," BMC Cell Biol. **8**, 40 (2007).
[100]B. Kesler, G. Li, A. Thiemicke, R. Venkat, and G. Neuert, "Automated cell boundary and 3D nuclear segmentation of cells in suspension," Sci. Rep. **9**, 10237 (2019).
[101]A. E. Carpenter, T. R. Jones, M. R. Lamprecht, C. Clarke, I. H. Kang, O. Friman, D. A. Guertin, J. H. Chang, R. A. Lindquist, J. Moffat *et al.*, "Cellprofiler: Image analysis software for identifying and quantifying cell phenotypes," Genome Biol. **7**, R100 (2006).
[102]C. McQuin, A. Goodman, V. Chernyshev, L. Kamentsky, B. A. Cimini, K. W. Karhohs, M. Doan, L. Ding, S. M. Rafelski, D. Thirstrup *et al.*, "Cellprofiler 3.0: Next-generation image processing for biology," PLoS Biol.ogy **16**, e2005970 (2018).
[103]C. Sommer, C. N. Straehle, U. Koethe, F. A. Hamprecht *et al.*, "Ilastik: Interactive learning and segmentation toolkit," in *IEEE International Symposium on Biomedical Imaging* (IEEE, 2011), Vol. 2, p. 230.
[104]Y. Toyoshima, T. Tokunaga, O. Hirose, M. Kanamori, T. Teramoto, M. S. Jang, S. Kuge, T. Ishihara, R. Yoshida, and Y. Iino, "Accurate automatic detection of densely distributed cell nuclei in 3D space," PLoS Comput. Biol. **12**, e1004970 (2016).
[105]M. Verschuuren, J. De Vylder, H. Catrysse, J. Robijns, W. Philips, and W. H. De Vos, "Accurate detection of dysmorphic nuclei using dynamic programming and supervised classification," PLoS One **12**, e0170688 (2017).
[106]P. Wang, X. Hu, Y. Li, Q. Liu, and X. Zhu, "Automatic cell nuclei segmentation and classification of breast cancer histopathology images," Signal Process. **122**, 1–13 (2016).
[107]S. Choi, W. Wang, A. J. Ribeiro, A. Kalinowski, S. Q. Gregg, P. L. Opresko, L. J. Niedernhofer, G. K. Rohde, and K. N. Dahl, "Computational image analysis of nuclear morphology associated with various nuclear-specific aging disorders," Nucleus **2**, 570–579 (2011).
[108]R. Hollandi, A. Szkalisity, T. Toth, E. Tasnadi, C. Molnar, B. Mathe, I. Grexa, J. Molnar, A. Balind, M. Gorbe *et al.*, "nucleAIzer: A parameter-free deep learning framework for nucleus segmentation using image style transfer," Cell Syst. **10**, 453–458 (2020).
[109]E. Arbustini, A. Pilotto, A. Repetto, M. Grasso, A. Negri, M. Diegoli, C. Campana, L. Scelsi, E. Baldini, A. Gavazzi *et al.*, "Autosomal dominant dilated cardiomyopathy with atrioventricular block: A lamin A/C defect-related disease," J. Am. Coll. Cardiol. **39**, 981–990 (2002).
[110]M. V. Zaragoza, L. Fung, E. Jensen, F. Oh, K. Cung, L. A. McCarthy, C. K. Tran, V. Hoang, S. A. Hakim, and A. Grosberg, "Exome sequencing identifies a novel LMNA splice-site mutation and multigenic heterozygosity of potential modifiers in a family with sick sinus syndrome, dilated cardiomyopathy, and sudden cardiac death," PLoS One **11**, e0155421 (2016).
[111]J. T. Lu, A. Muchir, P. L. Nagy, and H. J. Worman, "Lmna cardiomyopathy: Cell biology and genetics meet clinical medicine," Disease Models Mech. **4**, 562–568 (2011).
[112]M. Koda, G. Takemura, H. Okada, M. Kanoh, R. Maruyama, M. Esaki, Y. Li, S. Miyata, H. Kanamori, L. Li *et al.*, "Nuclear hypertrophy reflects increased biosynthetic activities in myocytes of human hypertrophic hearts," Circ. J. **70**, 710–718 (2006).
[113]I. Banerjee, J. Zhang, T. Moore-Morris, E. Pfeiffer, K. S. Buchholz, A. Liu, K. Ouyang, M. J. Stroud, L. Gerace, S. M. Evans *et al.*, "Targeted ablation of Nesprin 1 and Nesprin 2 from murine myocardium results in cardiomyopathy, altered nuclear morphology and inhibition of the biomechanical gene response," PLoS Genet. **10**, e1004114 (2014).
[114]E. Laurini, V. Martinelli, T. Lanzicher, L. Puzzi, D. Borin, S. N. Chen, C. S. Long, P. Lee, L. Mestroni, M. R. Taylor *et al.*, "Biomechanical defects and rescue of cardiomyocytes expressing pathologic nuclear lamins," Cardiovasc. Res. **114**, 846–857 (2018).
[115]V. G. Lockard and S. Bloom, "Trans-cellular desmin-lamin B intermediate filament network in cardiac myocytes," J. Mol. Cell. Cardiol. **25**, 303–309 (1993).
[116]M. K. Driscoll, J. L. Albanese, Z.-M. Xiong, M. Mailman, W. Losert, and K. Cao, "Automated image analysis of nuclear shape: What can we learn from a prematurely aged cell?," Aging **4**, 119 (2012).
[117]R. Mandelkow, D. Guembel, H. Ahrend, A. Kaul, U. Zimmermann, M. Burchardt, and M. B. Stope, "Detection and quantification of nuclear morphology changes in apoptotic cells by fluorescence microscopy and subsequent analysis of visualized fluorescent signals," Anticancer Res. **37**, 2239–2244 (2017).
[118]F. Nowzari, H. Wang, A. Khoradmehr, M. Baghban, N. Baghban, A. Arandian, M. Muhaddesi, I. Nabipour, M. I. Zibaii, M. Najarasl, P. Taheri, H. Latifi, and A. Tamadon, "Three-dimensional imaging in stem cell-based researches," Front. Vet. Sci. **8**, 657525 (2021).
[119]A. M. da Rocha, K. Campbell, S. Mironov, J. Jiang, L. Mundada, G. Guerrero-Serna, J. Jalife, and T. J. Herron, "hiPSC-CM monolayer maturation state determines drug responsiveness in high throughput pro-arrhythmia screen," Sci. Rep. **7**, 13834 (2017).
[120]F. Pampaloni, E. G. Reynaud, and E. H. K. Stelzer, "The third dimension bridges the gap between cell culture and live tissue," Nat. Rev. Mol. Cell Biol. **8**, 839–845 (2007).
[121]F. Piccinini, T. Balassa, A. Carbonaro, A. Diosdi, T. Toth, N. Moshkov, E. A. Tasnadi, and P. Horvath, "Software tools for 3D nuclei segmentation and quantitative analysis in multicellular aggregates," Comput. Struct. Biotechnol. J. **18**, 1287–1300 (2020).
[122]W. Han, S. Chen, W. Yuan, Q. Fan, J. Tian, X. Wang, L. Chen, X. Zhang, W. Wei, R. Liu, J. Qu, Y. Jiao, R. H. Austin, and L. Liu, "Oriented collagen fibers direct tumor cell intravasation," Proc. Natl. Acad. Sci. U. S. A. **113**, 11208–11213 (2016).
[123]Z. Liu, L. Speroni, K. P. Quinn, C. Alonzo, D. Pouli, Y. Zhang, E. Stuntz, C. Sonnenschein, A. M. Soto, and I. Georgakoudi, "3D organizational mapping of collagen fibers elucidates matrix remodeling in a hormone-sensitive 3D breast tissue model," Biomaterials **179**, 96–108 (2018).
[124]A. M. Greiner, H. Chen, J. P. Spatz, and R. Kemkemer, "Cyclic tensile strain controls cell shape and directs actin stress fiber formation and focal adhesion alignment in spreading cells," PLoS One **8**, e77328 (2013).
[125]A. Zemel, F. Rehfeldt, A. Brown, D. Discher, and S. Safran, "Optimal matrix rigidity for stress-fibre polarization in stem cells," Nat. Phys. **6**, 468–473 (2010).
[126]A. Bershadsky, M. Kozlov, and B. Geiger, "Adhesion-mediated mechanosensitivity: A time to experiment, and a time to theorize," Curr. Opin. Cell Biol. **18**, 472–481 (2006).
[127]T. Iba and B. E. Sumpio, "Morphological response of human endothelial cells subjected to cyclic strain *in vitro*," Microvasc. Res. **42**, 245–254 (1991).
[128]J. Pablo Rodríguez, M. González, S. Ríos, and V. Cambiazo, "Cytoskeletal organization of human mesenchymal stem cells (msc) changes during their osteogenic differentiation," J. Cell. Biochem. **93**, 721–731 (2004).
[129]S. K. Ghosh, "A model for the orientational order in liquid crystals," Il Nuovo Cimento D **4**, 229–244 (1984).
[130]B. T. Grys, D. S. Lo, N. Sahin, O. Z. Kraus, Q. Morris, C. Boone, and B. J. Andrews, "Machine learning and computer vision approaches for phenotypic profiling," J. Cell Biol. **216**, 65–71 (2017).

[131]J. Tan, C. Chua, K. Leong, K. Chian, W. Leong, and L. Tan, "Esophageal tissue engineering: An in-depth review on scaffold design," Biotechnol. Bioeng. **109**, 1–15 (2012).
[132]P. Camelliti, C. R. Green, and P. Kohl, "Structural and functional coupling of cardiac myocytes and fibroblasts," in *Cardiovascular Gap Junctions* (Karger Publishers, 2006), Vol. 42, pp. 132–149.
[133]C. A. Souders, S. L. Bowers, and T. A. Baudino, "Cardiac fibroblast: The renaissance cell," Circ. Res. **105**, 1164–1176 (2009).
[134]M. J. Ivey and M. D. Tallquist, "Defining the cardiac fibroblast," Circ. J. **80**, 2269 (2016).
[135]S. M. Biendarra-Tiegs, F. J. Secreto, and T. J. Nelson, "Addressing variability and heterogeneity of induced pluripotent stem cell-derived cardiomyocytes," in *Cell Biology and Translational Medicine* (Springer, 2019), Vol. 6, pp. 1–29.
[136]S. Berg, D. Kutra, T. Kroeger, C. N. Straehle, B. X. Kausler, C. Haubold, M. Schiegg, J. Ales, T. Beier, M. Rudy *et al.*, "ilastik: Interactive machine learning for (bio) image analysis," Nat. Methods **16**, 1226 (2019).
[137]J. C. Caicedo, S. Cooper, F. Heigwer, S. Warchal, P. Qiu, C. Molnar, A. S. Vasilevich, J. D. Barry, H. S. Bansal, O. Kraus *et al.*, "Data-analysis strategies for image-based cell profiling," Nat. Methods **14**, 849–863 (2017).
[138]M. Held, M. H. Schmitz, B. Fischer, T. Walter, B. Neumann, M. H. Olma, M. Peter, J. Ellenberg, and D. W. Gerlich, "CellCognition: Time-resolved phenotype annotation in high-throughput live cell imaging," Nat. Methods **7**, 747 (2010).
[139]S. Rajaram, B. Pavie, L. F. Wu, and S. J. Altschuler, "PhenoRipper: Software for rapidly profiling microscopy images," Nat. Methods **9**, 635–637 (2012).
[140]M.-A. Bray, S. Singh, H. Han, C. T. Davis, B. Borgeson, C. Hartland, M. Kost-Alimova, S. M. Gustafsdottir, C. C. Gibson, and A. E. Carpenter, "Cell painting, a high-content image-based assay for morphological profiling using multiplexed fluorescent dyes," Nat. Protocols **11**, 1757 (2016).
[141]J. Zhou, S. Lamichhane, G. Sterne, B. Ye, and H. Peng, "BIOCAT: A pattern recognition platform for customizable biological image classification and annotation," BMC Bioinf. **14**, 291 (2013).
[142]K. A. Gerbin, T. Grancharova, R. Donovan-Maiye, M. C. Hendershott, J. Brown, S. Q. Dinh, J. L. Gehring, M. Hirano, G. R. Johnson, A. Nath *et al.*, "Cell states beyond transcriptomics: Integrating structural organization and gene expression in hiPSC-derived cardiomyocytes," Cell Syst. **12**, 670 (2021).
[143]E. Meijering, A. E. Carpenter, H. Peng, F. A. Hamprecht, and J.-C. Olivo-Marin, "Imagining the future of bioimage analysis," Nat. Biotechnol. **34**, 1250–1255 (2016).